Research Article / Mechanical - Materials Engineering http://dx.doi.org/10.15446/ing.investig.v40n2.79469

A study of the stress field generated by the contact between a sphere and a flat plate for a simplified model of deep-groove ball bearing

Un estudio del campo de tensión generado por el contacto entre una esfera y una placa plana para un modelo simplificado de rodamientos rígidos de bolas

A. O. Köhn[1] and F. de A. Silva[2]

ABSTRACT

Bearings are mechanical elements capable of transferring motion between two or more parts in a machine. When an external load is applied, the rolling elements and their rings tend to initiate a cyclical movement between themselves. Hence, they are linked by a variable type of contact, thus creating high surface stresses. As these elements are subjected to millions of cycles within their lifespan, these cyclical stresses may create cracks and cause failure by rolling contact fatigue (RCF). Due to the importance of this subject, it is vital to study the stress field caused by contact between the rolling parts in a bearing. This paper offers two approaches on the cyclical stresses in a deep-groove ball bearing: an analytical approach, using Hertz's theory for contact stresses; and a numerical simulation, using the Finite Element Method (FEM) with the software *Inventor* and *Nastran In-CAD*. The results of both approaches were compared, and stress behavior was analyzed as the depth of the inner ring was increased. It was concluded that the surface stresses are greatly superior than the strength of the materials used in the bearings, and that the area influenced by these stresses are small when compared to the dimensions of the whole.

Keywords: Hertz contact stress, FEM model, deep-groove ball bearing, surface contact

RESUMEN

Los rodamientos son elementos mecánicos capaces de transferir movimiento entre dos o más partes en una máquina. Cuando se aplica una carga externa, los elementos rodantes y sus anillos tienden a iniciar un movimiento cíclico entre ellos. Por lo tanto, están vinculados por un tipo variable de contacto, creando altas tensiones superficiales. Como estos elementos están sujetos a millones de ciclos en su vida útil, estas tensiones cíclicas pueden crear grietas y causar fallas debido a la fatiga por contacto. Debido a la importancia de este tema, es vital estudiar el campo de tensión causado por el contacto entre las partes rodantes en un rodamiento. Este documento ofrece dos enfoques sobre las tensiones cíclicas en un rodamiento rígido de bolas: un enfoque analítico, utilizando la teoría de Hertz para las tensiones de contacto; y una simulación numérica, utilizando el Método de Elementos Finitos con el software *Inventor* y *Nastran In-CAD*. Los resultados de ambos enfoques se compararon y se analizó el comportamiento de las tensiones a medida que aumentaba la profundidad del anillo interior. Se llegó a la conclusión de que las tensiones superficiales son muy superiores a la resistencia de los materiales utilizados en los rodamientos, y que el área influenciada por estas tensiones es pequeña en comparación con las dimensiones del conjunto.

Palabras clave: estrés por contacto de Hertz, modelo FEM, rodamiento rígido de bolas, contacto superficial

Received: May 5th, 2019
Accepted: April 22th, 2020

Introduction

Bearings are mechanical elements used in the naval, aeronautical, automotive and various others branches of the industry. These are crucial elements in the transmission of motion between two parts – for example, a bearing and a shaft. A good bearing performance requires a combination of different parameters acting simultaneously on the element, such as rotation speed, applied loads, lubrication, and geometry of the parts involved in the contact.

Bearings are defined by the type of their rolling elements (balls, needles, rollers, etc), number of rows (single, double, triple), and the type of applied load (radial and/or axial) (Norton,

[1]Mechanical Engineer, Universidade Estadual Paulista (UNESP), Brazil. Affiliation: Mastering Student, Universidade Estadual Paulista (UNESP), Brazil.
E-mail: andre.oliveira.kohn@gmail.com
[2]Mechanical Engineer, Universidade Católica de Petrópolis, Brazil. Ph.D. Mechanical Engineering, Universidade Estadual de Campinas (UNICAMP), Brazil. Affiliation: Associate Professor, Universidade Estadual Paulista (UNESP), Brazil.
E-mail: fernando.azevedo@unesp.br

How to cite: A. O. Kohn and F. de A. Silva (2020). A study of the stress field generated by the contact between a sphere and a flat plate for a simplified model of deep-groove ball bearing. *Ingeniería e Investigación*, *40*(2), 37-42. 10.15446/ing.investig.v40n2.79469

2013). The bearing type is chosen based on the conditions and requirements of its application. These machine elements are usually formed by steel rolling elements between two rings (inner and outer), which are retained within a cage.

When an external load initiates rotation, surface contact stresses may cause a subsurface crack, which can grow until it reaches the surface. This endangers the bearing, risking failures such as pitting and spalling, which can compromise the whole machine and cause great financial and human loss.

Due the importance of this matter, many papers seek to understand the mechanism of this problem. However, the study of contact between bearing parts is known to be a complex issue, since the contact area is subjected to stresses as high as 2~5 GPa (Norton, 2013; Rycerz, Olver, and Kadiric, 2017; Morales-Espejel and Gabelli, 2015; Bhattacharyya, Londhe, Arakere, and Subhash, 2017; Li, Hu, Meng, Zhan, and Shen, 2017 Arakere, 2016), as well as several other parameters that have an impact on the situation, such as lubrication, vibration, roughness (Yusof and Ripin, 2014), bearing dimensions (Chen and Wen, 2015), rotation speed, applied loads (Guo, Cao, He, and Yang, 2015), and the curvature of the inner and outer rings (Deng, Hua, Han, and Huang, 2013; Chen and Wen, 2015). Therefore, each parameter must be examined thoroughly, seeking to determine the influence of its behavior on RCF.

Contact between the rolling element and the race creates a triaxial compressive stress field, along with shear stresses in all directions (Bhattacharyya et al., 2017; Arakere, 2016). Many studies showed that shear stresses are responsible for the appearance of cracks (Bhattacharyya et al., 2017; Juvinall and Matshek, 2008; Deng, Hua, Han and Huang, 2014). Studies like Deng, Hua, Han, Wei and Huang (2015) and Deng, Hua, Han and Huang (2013) showed that there will be a peak of stresses around a subsurface material defect, initiating a crack that will spread until it reaches the surface, causing failure of the element.

RCF has a different behavior in each type of bearing, due to the difference in their contact geometry. Morales-Espejel (2014) and Deng et al. (2014) discussed the phenomenon in roller bearings, whereas Li et al. (2017) examined the performance of tapered roller bearings, and Lostado, Martinez, and Donald (2015) studied self-aligning roller bearings. This paper proposes a simplified model for a deep-groove ball bearing.

Neglecting the lubrication effects, the analytical approach for this problem is based on the Hertz equations for contact surfaces (Chen and Wen, 2015). To validate the results, it is crucial to apply the numerical method and a FEM software to obtain the stress field (Lostado et al., 2015). Comparing both approaches, it is possible to achieve a number close to reality.

The contact seen in a deep-groove ball bearing can be simplified using a sphere and flat plane (Norton, 2013). In this paper, the stress field caused by this type of contact was calculated and analyzed. The analysis was performed by using the Hertz equations for contact stress, and these results were compared to the data obtained from the numerical method, using FEM software *Nastran in-CAD* and *Inventor*.

Theoretical analysis

In a deep-groove ball bearing, the rolling elements are in contact with the inner and outer races. When an external load is applied, these balls tend to roll over the race, allowing the transmission of motion between them. This movement consists of 99% rolling and 1% sliding (Norton, 2013).

The contact area is directly related to the geometry and mechanical properties of the materials in contact. Ideally, the contact between a sphere and a flat plate would be represented with a single point with no dimension, generating an infinite stress. However, the applied load causes a small deformation, creating a small contact area with radius a, minimal when compared to the radius of the sphere, causing high compressive stresses. Hence, a high stress field is generated, which may lead to RCF failure of the element. These stresses are much higher than the strength of the materials used in bearings, reaching 2~5 GPa. Figure 1 illustrates the contact area between a sphere and a flat plate in a simplified manner.

Each part of the ball will have touched the race after a rotation is completed. Therefore, this movement creates cyclical stresses described as Hertz stresses (Norton, 2013), thus inducing the formation of pits and spalls and, consequently, complete failure by RCF.

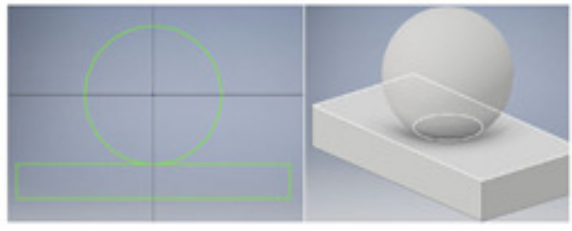

Figure 1. Circular contact zone between a sphere and a flat plate.
Source: Authors

Hertz's stress theory takes into consideration some parameters like surface geometry of the bodies in contact, mechanical properties (Young's Modulus and Poisson ration), and applied loads. Therefore, it is possible to calculate shear and normal stress.

When considering two spheres, Norton (2013) and Juvinall and Matshek (2008) state that the stress between them is dependent on the material and geometrical constants of each sphere. The first is shown in Equation (1), where n is the index that defines each element; and the second is referred to in Equation (2) and involves the curvature of both spheres (R_1 e R_2).

$$m_n = \frac{1 - \upsilon_n{}^2}{E_n} \tag{1}$$

$$b = \left(\frac{1}{2}\right)\left(\frac{1}{R_1} + \frac{1}{R_2}\right) \tag{2}$$

According to Norton (2013) and Juvinall and Matshek (2008), the maximum pressure is seen at the center of the contact region, and P_{mean} is the mean pressure obtained through the division between the applied load F and the contact area of radius a, which is obtained through Equation (5).

$$P_{max} = \frac{3}{2}\frac{F}{\pi a^2} \tag{3}$$

$$P_{mean} = \frac{F}{\pi a^2} \tag{4}$$

$$a = 0,375\sqrt[3]{\frac{m_1 + m_2}{B}F} \tag{5}$$

The applied load F will create a triaxial stress field, in which σ_x, σ_y e σ_z are all compressive and whose maximum is found at the surface. They decrease progressively as the depth is increased (Norton, 2013). The maximum stresses are, at the same time, the main stresses (Juvinall and Matshek 2008).

According to Norton (2013), it is possible to describe the behavior of the shear and the three main normal stresses with Equations (6-8). Plane xy is the one that contains the region of contact between the two surfaces, and z, which represents depth, is the perpendicular axis of this plane.

$$\sigma_x = \sigma_y = \frac{P_{max}}{2}\left[-(1+2\upsilon) + 2(1+\upsilon)\left(\frac{z}{\sqrt{(a^2+z^2)}}\right) + \cdots - \left(\frac{z}{\sqrt{(a^2+z^2)}}\right)^3\right] \tag{6}$$

$$a = 0,375\sqrt[3]{\frac{m_1 + m_2}{B}}F\sigma_z = P_{max}\left[-1 + \frac{z^3}{(a^2+z^2)^{\frac{3}{2}}}\right] \tag{7}$$

$$\tau_{xz} = \tau_{yz} = \frac{P_{max}}{2}\left[\frac{(1-2\upsilon)}{2} + (1-\upsilon)\left(\frac{z}{\sqrt{(a^2+z^2)}}\right) + \cdots - \left(\frac{3}{2}\right)\left(\frac{z}{\sqrt{(a^2+z^2)}}\right)^3\right] \tag{8}$$

Materials and methods

Analytical approach

The calculation was based on a deep-groove ball bearing, from the manufacturer FAG, series 6207. Table 1 shows the dimensions used in Equations (1-9) and Figure 2 illustrates the sectional drawing of a bearing.

The applied load was calculated based on the guidelines for an electric rotor project. The total load applied on the bearing was F = 1 010,6 N. The used model has nine balls, as illustrated in Figure 3. Therefore, it is necessary to divide the total load by the number of rolling elements, thus obtaining 112,3 N. This value was applied to Equations (3-8) to obtain the stress field from the contact surface.

Table 1. Bearing dimensions

Dimensions	Measure
d	35,0 mm
D	72,0 mm
B	17,0 mm
d_1	47,2 mm
D_1	60,7 mm
D_{sphere}	11,0 mm

Source: Authors

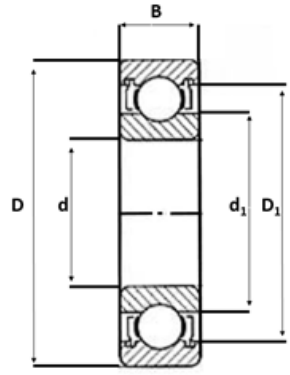

Figure 2. Sectional drawing of bearing.
Source: Authors

Figure 3. Deep-groove ball bearing FAG 6 207.
Source: Authors

As it was mentioned above, the contact region of the ball and race is complex, since it has 4 different curvatures (one radial and one axial for each element). In order to simplify the calculations, it was assumed that one of the bodies is a flat plate. In this case, R_2 tends to infinity, making the Hertz equations easier to calculate. Despite this simplification, the results are still valid and realistic (Norton, 2013).

It was defined that the bearing is made of AISI 52100, the most common steel alloy for this type of operation (Chen and Wen, 2015). Table 2 shows all values used in the calculations.

Using the values from Table 2, the results for B, P_{max}, P_{mean}, as well as stresses σ_x, σ_y, σ_z, τ_{xz} and τ_{yz} were obtained from Equations (3-8). As the maximum normal stresses are observed at the contact plane of the two bodies, z must be zero, or in other words, the depth must equal zero.

Table 2. Values of the parameters used

Sphere Radius	R_1	5,5 mm
Plate Radius	R_2	∞
Young's Modulus (sphere)	E_1	210,0 GPa
Young's Modulus (plate)	E_2	210,0 GPa
Poisson's Ratio (sphere)	υ_1	0,3
Poisson's Ratio (plate)	υ_2	0,3
Applied load in each sphere	F	112,3 N

Source: Authors

Numerical approach

According to Bhattacharyya et al. (2017) and Satyanarayana and Melkote (2004), the contact between a sphere and a flat plate can be simplified to ¼ of the model due to the contact symmetry, thus maintaining the same characteristics of whole model. Therefore, a computational ¼ model of the sphere and the flat plate (which represents the inner ring of the bearing) was constructed by means of the FEM software *Inventor* and *Nastran in-CAD,* as seen in Figure 4.

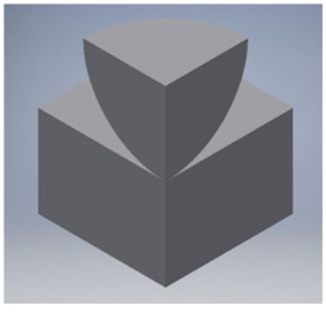

Figure 4. ¼ model of the sphere and flat plate.
Source: Authors

Constraints

The lower side of the flat plate was fixed with constraints in all directions.

In order to simulate the symmetry of the complete model, symmetry constraints in relation to the axes x and y for the internal faces of the sphere and plate were applied. Therefore, the simplified model behaves exactly as its complete version.

Loads

A compressive load of 112,3 N was applied on the upper side of the sphere. This value represents the load that each sphere receives when a total external load of 1 010,6 N is applied.

Mesh

The mesh was automatically generated by the software. However, it was necessary to refine it at the contact vertex between the sphere and the plate, in order to obtain more precise results.

The final mesh was made with parabolic elements, sized 0,626441 mm, with a tolerance of 1,25288e-05, and it has 6 903 nodes and 4 299 elements.

Surface contacts

The external surface of the sphere is in contact with the upper side of the flat plate. To model according to reality, the option *Sliding/ No Separation* was used for this contact. Hence, it is defined that the parts will not be allowed to separate and will keep attached during the whole operation.

Results and discussion

As it was mentioned before, the contact between the sphere and the race can be simplified to a sphere and flat plate model, and when an external load is applied, a triaxial stress field is created. The shear stresses can cause the appearance of subsurface cracks which may reach the surface, thus causing the failure of the bearing.

With the values mentioned in section 3, it was possible to begin with the analytical and numerical approaches. The results are displayed in Table 3, where a percentage deviation between the results is also presented, in order to show the percentage difference from the stresses obtained by both approaches. All results in Table 3 are located at $z = 0$ and correspond to the maximum values found in the model.

Table 3. Analytical and numerical results

	Analytical (MPa)	Numerical (MPa)	Percentage deviation
σ_x	-1 698,14	-1 667,04 MPa	2%
σ_y	-1 698.14	-1 645,38 MPa	3%
σ_z	-2 122,68	-3 617,99 MPa	70%
τ_{yz}	706,66	682,80 MPa	3%
τ_{xz}	706,66	696,62 MPa	1%

Source: Authors

Analytical results

Applying the parameters previously mentioned in the Equations (3-8), the results for the five maximum stresses were obtained, as indicated in Table 3. The radius of the contact circumference is 0,159 mm, and the contact area between the bodies is 0,0793 mm^2.

As expected, all normal stresses are compressive. The stresses in directions x and y have the same behavior, and they are both in the contact plane of the bodies. The stress in the direction z has maximum values. The shear stresses from planes yz and xz have the same values, and they are both perpendicular to the contact plane of the sphere and the plane. All maximum normal stresses are found in the contact region, that is, where $z = 0$ and the depth is null, as expected. As the depth increases, the stress decreases until it reaches zero.

In order to analyze how these stresses behave as the depth increases, the chart in Figure 5 was created with Equations (6-8). The horizontal axis represents the depth z divided by the constant value of the radius a, and the vertical axis represents the stresses divided by the constant value of P_{max}.

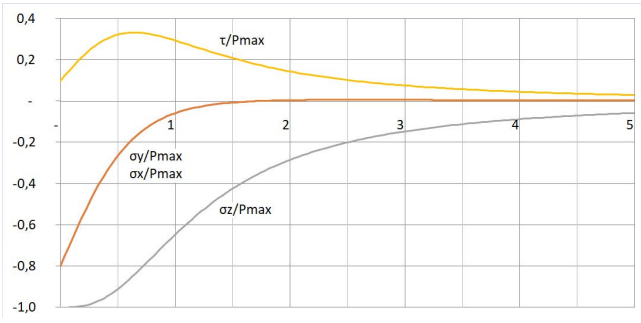

Figure 5. Behavior of the stresses as a function of depth.
Source: Authors

Figure 5 shows that σ_x and σ_y have the same behavior. The maximum stresses are located at $z = 0$ and have values around 0,8 P_{max}. These stresses fall quickly as the depth increases. When the depth reaches approximately 1,5x the value of a, σ_x and σ_y become null.

The maximum stress σ_z has the same value as P_{max}, and its curve declines softer than the stresses in the direction of x and y. Its value tends to zero just when the depth reaches around 5x the value of the radius a.

The maximum shear stress is found under the surface, at approximately $z = 0{,}63a$, and its value is around 0,33 P_{max}.

Consequently, it is possible to conclude that the stresses vary significantly in a small region. For a depth 5x bigger than the circumference radius from the contact area, all stresses are reduced to less than 10% of their maximum value. Thus, it is concluded that the measurement and study of these stresses is a complex subject, since stresses vary drastically within a millimeter region and, moreover, they have considerably high values. The normal stress peak is located at the contact of the bodies, and its values can reach 2 GPa.

Numerical results

Resolving the numerical simulation proposed in the item 3.2, the values of σ_x, σ_y, σ_z, τ_{yz} e τ_{xz} are obtained, as indicated in Table 3.

All maximum normal stresses are located at the vertex of the sphere and plate. Figure 6 shows that the critical point of this simulation for normal stresses is found at the vertex, and, as the depth is increased, this value decreases until it reaches zero. It is also seen that the region affected by the contact stresses is resumed to a small vicinity around the contact vertex.

By comparing the results from the numerical simulation and the analytical data, it can be seen that the results for σ_x, σ_y, τ_{yz} e τ_{xz} are significantly close between the two approaches, and its percentage deviation is around 2%.

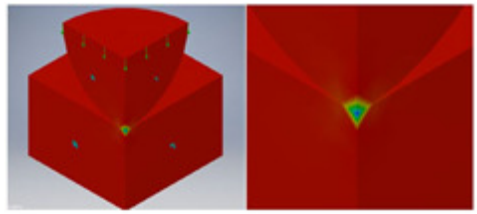

Figure 6. Numerical Result.
Source: Authors

However, the numerical value obtained for σ_z is relatively far from the analytical value.

Four out of five stresses calculated with the FEM software were validated by the analytical calculation. The discrepancy between the values obtained for σ_z can be justified by the inaccuracy from the Hertz equations regarding the thickness of the bodies, that is, the Equations (3-8) do not consider the thickness of the plate. Therefore, the FEM simulation can produce imprecise results compared to the analytical values.

Despite the discrepancy seen in one of the stresses, the theory says that shear stresses are the critical regarding the appearance of cracks that will cause the failure by RCF in the mechanical element. As the percentage deviation seen for this type of stress is around 2%, the FEM model can be validated for this simulation.

Conclusions

The study of the stresses caused by the cyclical contact between a sphere and the race of a deep-groove ball bearing are of high importance, especially regarding the RCF phenomenon. The cyclical contact between the bodies creates a complex high stress field (2~5 GPa), and this process can lead to total failure of the mechanical element.

In this paper, an analytical approach was proposed to study the contact between a sphere and a flat plate, using the Hertz theory for contact surfaces. A numerical method through a FEM model, using the software *Inventor* and *Nastran in-CAD*, was also proposed. The normal stresses obtained by both approaches were always compressive, and their maximum was located at the surface of the bodies. When the depth was increased, these stresses decreased quickly until they reached zero. Therefore, it can be concluded that the region affected by contact stresses is limited to a small vicinity around the contact vertex.

The results of both approaches were satisfactory. In spite of the divergence between the results for the normal stress perpendicular to the contact plane, the shear stresses obtained were similar for both methods, and these types of stresses are the most critical in the appearance of cracks.

Acknowledgements

This study was partially financed by the Conselho Nacional de Desenvolvimento Científico e Tecnológico (CNPq) and

Coordenação de Aperfeiçoamento de Pessoal de Nível Superior - Brasil (CAPES) - Finance Code 001.

References

Arakere, N. K. (2016). Gigacycle rolling contact fatigue of bearing steels: A review. *International Journal of Fatigue, 93*, 238-249. 10.1016/j.ijfatigue.2016.06.034

Bhattacharyya, A., Londhe, N., Arakere, N., and Subhash, G. (2017). A new approach towards life prediction of case hardened bearing steels subjected to rolling contact fatigue. *Materials Performance and Characterization, 6*(4), 656-677. 10.1520/MPC20160099

Chen, G., and Wen, J. (2015). Effects of size and raceway hardness on the fatigue life of large rolling bearing. *Journal of Mechanical Science and Technology, 29*(3), 3873-3883. 10.1007/s12206-015-0833-3

Chen, L., Xia, X. T., Zheng, H. T., and Qiu, M. (2016). Rework solution method on large size radial roller bearings. *Journal of the Brazilian Society of Mechanical Sciences and Engineering, 38*(4), 1249-1260. 10.1007/s40430-015-0364-y

Deng, S., Hua, L., Han, X., and Huang, S. (2013). Finite element analysis of fatigue life for deep groove ball bearing. *Proceedings of the Institution of Mechanical Engineers, Part L: Journal of Materials: Design and Applications*, *227*(1), 70-81. 10.1177/1464420712445968

Deng, S., Hua, L., Han, X., and Huang, S. (2014). Investigation of rolling contact fatigue cracks in ball bearings. *International Journal of Fracture, 188*(1), 71-78. 10.1007/s10704-014-9947-3

Deng, S., Hua, L., Han, X., Wei, W., and Huang, S. (2015). Analysis of surface crack growth under rolling contact fatigue in a linear contact. *Tribology Transactions, 58*(3), 432-443. 10.1080/10402004.2014.983250

Guo, W., Cao, H., He, Z., and Yang, L. (2015). Fatigue life analysis of rolling bearings based on quasistatic modeling. *Shock and Vibration, 2015*. 10.1155/2015/982350

Juvinall, R. C. and Matshek, K. M. (2008). *Fundamentos do projeto de componentes de máquinas*. Grupo Gen-LTC.

Li, F., Hu, W., Meng, Q., Zhan, Z., and Shen, F. (2017). A new damage-mechanics-based model for rolling contact fatigue analysis of cylindrical roller bearing. *Tribology International, 120*, 105-114. 10.1016/j.triboint.2017.12.001

Lostado, R., Martinez, R. F., and Mac Donald, B. J. (2015). Determination of the contact stresses in double-row tapered roller bearings using the finite element method, experimental analysis and analytical models. *Journal of Mechanical Science and Technology, 29*(11), 4645-4656. 10.1007/s12206-015-1010-4

Mohd Yusof, N. F., and Ripin, Z. M. (2014). Analysis of surface parameters and vibration of roller bearing. *Tribology Transactions, 57*(4), 715-729. 10.1080/10402004.2014.895887

Morales-Espejel, G. E., and Gabelli, A. (2015). The progression of surface rolling contact fatigue damage of rolling bearings with artificial dents. *Tribology Transactions, 58*(3), 418-431. 10.1080/10402004.2014.983251

Norton, R. L. (2013). *Projeto de máquinas*. (4th Edition). Bookman Editora. Porto Alegre, Brazil.

Rycerz, P., Olver, A., and Kadiric, A. (2017). Propagation of surface initiated rolling contact fatigue cracks in bearing steel. *International Journal of Fatigue, 97*, 29-38. 10.1016/j.ijfatigue.2016.12.004

Satyanarayana, S., and Melkote, S. N. (2004). Finite element modeling of fixture–workpiece contacts: single contact modeling and experimental verification. *International journal of machine tools and manufacture, 44*(3), 903-913. 10.1016/j.ijmachtools.2004.02.010